

September 2, 2011

# First observation of trapped high-field seeking ultracold neutron spin states.

M. Daum<sup>1,2,3,a</sup>, P. Fierlinger<sup>2</sup>, B. Franke<sup>1,2</sup>, P. Geltenbort<sup>4</sup>, L. Goeltl<sup>1</sup>,  
E. Gutmiedl<sup>2</sup>, J. Karch<sup>5</sup>, G. Kessler<sup>2</sup>, K. Kirch<sup>1,6</sup>, H.-C. Koch<sup>5</sup>, A. Kraft<sup>5</sup>,  
T. Lauer<sup>5</sup>, B. Lauss<sup>1</sup>, E. Pierre<sup>7</sup>, G. Pignol<sup>8</sup>, D. Reggiani<sup>1</sup>, Yu. Sobolev<sup>5</sup>,  
T. Zechlau<sup>5</sup>, G. Zsigmond<sup>1</sup>

<sup>1</sup>PSI, Paul-Scherrer-Institut, CH-5232 Villigen PSI, Switzerland.

<sup>2</sup>TUM, Physik-Department Technische Universität München, Excellence Cluster Universe, Munich, Germany.

<sup>3</sup>Department of Physics, University of Virginia, Charlottesville, VA22904-4714, USA.

<sup>4</sup>ILL, Institut Laue-Langevin, Grenoble, France.

<sup>5</sup>Institut für Physik, Johannes-Gutenberg-Universität, Mainz, Germany.

<sup>6</sup>IPP, Institut f. Teilchenphysik, ETH Zürich, CH-8093 Zürich, Switzerland.

<sup>7</sup>LPC, Laboratoire de Physique Corpusculaire, ENSICAEN-CNRS/IN2P3, Caen, France.

<sup>8</sup>LPSC, Laboratoire de Physique Subatomique et de Cosmologie, UJF-CNRS/IN2P3-INPG, Grenoble, France.

## Abstract

Ultracold neutrons were stored in a volume, using a magnetic dipole field shutter. Radial confinement was provided by material walls. Low-field seeking neutrons were axially confined above the magnetic field. High-field seeking neutrons are trapped inside the magnetic field. They can systematically shift the measured neutron lifetime to lower values in experiments with magnetic confinement.

### **PACS numbers:**

29.25.Dz Neutron sources, 28.20.-v Neutron physics, 14.20.Dh Protons and neutrons

### **Key words:**

Ultracold neutrons, ultracold neutron storage, neutron lifetime

<sup>a</sup>Corresponding author:

Tel.: +41 56 310 3668, fax +41 56 310 3294, e-mail: manfred.daum@psi.ch

## 1. Introduction

The free neutron interacts via all known forces. While the weak interaction is responsible for the decay of the neutron, e.g.,  $n \rightarrow p + e^- + \bar{\nu}_e$ , strong interaction, gravity, and electromagnetic interaction can be used to store very slow neutrons with velocities  $v_n \leq 7$  m/s in bottles. These neutrons are termed ultracold neutrons, UCN, because a neutron gas with such neutron velocities has a temperature below 3 mK.

The coherent strong interaction potential arises in the theoretical treatment of the interaction of very low energy neutrons (with their corresponding large neutron wave length) with materials in terms of refraction, see, e.g., Ref. [1]. As a consequence, the interaction of neutrons with material surfaces [2–4] can be described by a potential,  $V_f = V - iW$ . Here,  $V$  and  $W$  depend on the nuclear properties of the surface atoms:

$$V = \frac{2\pi\hbar^2}{m} \cdot N \cdot b; \quad W = \frac{\hbar}{2} \cdot N \cdot \sigma \cdot v, \quad (1)$$

where,  $m$  denotes the neutron mass,  $N$  the scattering centre density,  $b$  the bound coherent nuclear scattering length,  $\sigma$  the loss cross section per atom of the surface material,  $\hbar$  Planck's constant, and  $v$  the neutron velocity. For neutrons being reflected from a material surface the real part of the potential,  $V$ , sets the critical velocity,  $v_c = \sqrt{2V/m}$ , for total reflection and the imaginary part,  $W$ , determines the reflection loss [5, 6].

Ultracold neutrons interact with the gravitational field of the Earth. Their potential energy per height,  $E_{\text{pot}}/h = m \cdot g$ , is equivalent to 102 neV/m. That means an UCN of 250 neV corresponding to a velocity of about 7 m/s can rise against the Earth's gravitational field to about 2.5 m.

When a neutron enters a magnetic field  $B$  it is reflected if the orientation of its magnetic moment is antiparallel to the direction of the magnetic field and if its kinetic energy is  $E \leq E_B = |1.91 \cdot \mu_N \cdot B| = 60 \text{ neV/T} \cdot B$ , with  $\mu_N$  the nuclear magneton. Because of the repulsion, neutrons with this spin orientation are generally termed low-field seekers, LFS. Neutrons with the orientation of the magnetic moment parallel to the field are accelerated into the magnetic field with the force  $F_m = -\nabla[\mu \cdot B] = |\mu|\nabla|B|$  and are therefore termed high-field seekers, HFS. This assumes that the neutron's motion is so slow that its magnetic moment always keeps the same orientation with respect to the magnetic field (adiabatic case). The condition for this is that the time variation, i.e., the rotation rate of the magnetic field  $B$  seen by the neutron as it moves through the inhomogeneous field is much less than the

Larmor frequency,  $\omega_L$ , of the neutron spin:

$$\frac{|d\vec{B}_\perp/dt|}{B} = \frac{|d\vec{B}_\perp/dx| \cdot |dx/dt|}{B} \ll \omega_L = \frac{2 \cdot \mu_n}{\hbar} \cdot B. \quad (2)$$

Here,  $d\vec{B}_\perp/dx$  is the magnetic field gradient perpendicular to  $\vec{B}$ ,  $|dx/dt|$  the neutron velocity, and  $\mu_n$  the neutron magnetic moment,  $\mu_n = -1.91 \cdot \mu_N$ .

Ultracold neutron storage in a multipole magnetic field has been used in the past to measure the lifetime of the free neutron [10, 11]. Because of discrepancies in the most precise neutron lifetime measurements [12–14], new experiments with magnetic confinement in order to avoid losses on wall collisions are in discussion worldwide.

## 2. Experimental apparatus

Our apparatus for the storage of UCN takes advantage of all interactions (except the weak interaction) neutrons participate in, (i) the coherent strong interaction of neutrons with a material wall, (ii) gravitation and (iii) the electromagnetic force. The apparatus is shown in Fig. 1 and described in detail in Ref. [15].

We have recently performed an experiment to measure the depolarisation of UCN in neutron guides [16] at the beam line PF2/EDM [17, 18] of the Institute Laue-Langevin (ILL), Grenoble. Ultracold neutrons from the UCN turbine [19] enter the experimental apparatus from the right through an UCN guide (1, Fig. 1) and a rotatable shutter (2, Fig. 1) in open position. With the UCN switch (4, Fig. 1) in filling position, UCN are deflected into a cylindrical vertical neutron guide (6 and 16, Fig. 1) which is placed in a bore through the centre of the iron yokes and poles of the magnet. It is 1.5 m long, has an outer diameter of 80 mm, an inner diameter of 70 mm, and is coated with a 500 nm thick layer of materials with high optical potential, e.g. Ni/Mo alloy with a weight ratio of 85 % Ni and 15 % Mo (NiMo 85/15). This alloy is non-magnetic [20] and has an optical potential of 238 neV [5] which makes it well suited for the transport of polarised as well as unpolarised UCN.

Our coordinate system is defined as follows: The origin is placed in the midplane of the air gap and the center of the bore in the H-type split coil magnet, with the height  $z = 0$  and the radius  $r = 0$ . The upper 900 mm of the sample tube (16, Fig. 1) are above the air gap of the H-type split coil magnet, i.e., at  $z > 0$ , and serve as a storage volume for UCN. The H-type split coil magnet is used to make a dipole field at the lower end of the storage volume. Ultracold neutrons are filled into the storage volume with the magnetic field switched off. After 20 s of filling, equilibrium neutron density in the storage volume is reached and the magnetic field

in the air gap is switched on for the storage of UCN. The field is raised within about 2 s to 90 % of the maximum electric current resulting in a magnetic field strength of 1.45 T and corresponding to an UCN kinetic energy of 87 neV at the origin of the coordinate system. Then, the mechanical neutron switch (4, Fig. 1) is moved from filling position to emptying position into the detector (3, Fig. 1) blocking UCN from the turbine. The beam line shutter (2, Fig. 1) is closed for improved background suppression.

After switching on the magnetic field, the stored UCN spectrum is “cleaned” by waiting without any action over a time of 100 s. This period was found by Monte-Carlo calculations using GEANT4UCN [21] and by experimentally varying this time span. With the absorber position at 890 mm during this cleaning period, all UCN in the storage volume above the magnetic field with kinetic energies higher than 87 neV at  $z = 0$  have been either absorbed at the absorber or have penetrated the magnetic field downwards and have fallen into the neutron counter (3, Fig. 1), where they have been absorbed and detected. Low-field seekers with energies below 87 neV at  $z = 0$  are stored in the storage volume. For absorber positions lower than 890 mm, the storable LFS energies change accordingly. High-field seekers in the storage volume above the magnetic field are either absorbed on top or penetrate the magnetic field and fall into the detector.

After the spectral cleaning time of 100 s, the magnet current is raised in a split second ( $t \sim 0.3$  s) to 100 %, resulting in 1.5 T and UCN are stored over holding times reaching from 20 to 370 s. Neutrons which have been spin-flipped during these holding times, e.g., by interaction with the wall material during a wall bounce, can now pass the magnetic shutter and are registered in the neutron detector. After storage, the magnetic field is rapidly switched off ( $t < 2$  s) and the remaining UCN are detected over an emptying time of 45 s. Figure 2 shows the detector counts over time from filling (detector closed), spectral cleaning, storage and emptying. With this procedure, the wall loss and depolarisation probabilities of UCN interacting with the material of the wall can be determined, cf. Refs. [22, 23].

### 3. UCN energy distribution in the storage volume

In order to study eventual energy dependences of the UCN loss and depolarisation probabilities - the results will be presented later elsewhere in Ref. [16] - the experimental cycle shown in Fig. 2 has been performed with the absorber (15, Fig. 1) at different heights. The maximal storable UCN energy is then defined by the absorber height. Figure 3 shows the UCN counts in the emptying period as a function

of the UCN absorber height. The number of UCN counts decreases continuously between the absorber positions at  $z = 890$  mm and  $z = 400$  mm. Between  $z \sim 300$  mm and  $z \sim 100$  mm, the UCN counts are constant at a level of about 7 % of the total counts and decrease to zero at zero height position. This means that there are no or only very few UCN in the storage volume between  $z \sim 100$  mm and  $z \sim 300$  mm, as one can easily see from the differential energy spectrum, Fig. 3. This finding is confirmed by the potential energy distribution of UCN in the apparatus, see Fig. 4. The calculation is based on magnetic field measurements along the vertical axis of the apparatus and two-dimensional rotation-symmetric field distribution calculations using the code POISSON SUPERFISH [24].

The explanation of this phenomenon is as follows: There are quite some UCN traversing the region of the magnetic field while the field is ramped rapidly. Those with their magnetic moments antiparallel to the magnetic field (LFS) are accelerated out of the magnetic field region into the storage volume and experience a gain in total energy. They can be stored if their kinetic energy after this acceleration is below 87 neV at  $z = 0$ . This energy corresponds to the 1.45 T magnetic field during the ‘spectral cleaning’. High-field seekers are decelerated and trapped in the high magnetic field region if their kinetic energy at  $z = 0$  is smaller than about 10 neV immediately after the magnetic field of 1.45 T is switched on.

Further measurements have been performed using samples coated with Ni alloys which are ferromagnetic at room temperature, e.g., NiMo 91/9, NiMo 94/6, and natural nickel. These samples are probably immediately magnetised to saturation in the vicinity of the magnet air gap when the magnetic field is switched on.

For the stored HFS, the depolarisation rate is very small and almost equal to the background. At the inner radius of the cylindrical vertical neutron guide, i.e., where the material under investigation is coated onto the cylinder wall, the magnetic field in the midplane of the air gap,  $z = 0$ ,  $r = 35$  mm, is about 2.1 T, see Fig. 5. At this field value, the ferromagnetic Ni coating is in saturation with the relative permeability  $\mu = 1$  for  $B > 0.6$  T. The magnetic field gradient here is  $d\vec{B}_\perp/dx \approx (0.7 \text{ T})/(0.035 \text{ m}) = 20 \text{ T/m}$ . At  $E_{\text{kin}}(\text{max}) = 87 \text{ neV}$  the velocity of UCN is  $v_n(\text{max}) = 4.1 \text{ m/s}$ . For the HFS, however, it is more like  $v_n(\text{max}) = 2 \text{ m/s}$  and  $(d\vec{B}_\perp/dt)/B = 16.7 \text{ Hz}$ . The Larmor frequency is, cf. Eq. 2,  $\omega_L \approx 4 \cdot 10^8 \text{ Hz}$ . Here, the adiabatic condition for the neutron spin orientation to follow the magnetic field lines, cf. Eq. 2, is well fulfilled and the neutron spin orientation is not changed because the magnetisation in the scatter material is parallel to the neutron magnetic moment. From a measurement at different absorber heights, one can see that all the stored

HFS in a magnetic sample are confined within  $z \sim 130$  mm above (and below) the vertical centre of the dipole field in the air gap of the magnet, see Fig. 6.

In the case of changing the magnetic field after the cleaning period from 1.45 T to 1.52 T at the origin of the coordinate system,  $z = 0$ ,  $r = 0$ , in a split second ( $\sim 0.3$  s) we obtain  $(d\vec{B}_\perp/dt)/B = (0.05 \text{ T})/(0.3 \text{ s})/(1.5 \text{ T}) = 1.1 \text{ Hz}$ . Also here the adiabatic condition, cf. Eq. 2, is well fulfilled and no depolarisation can occur due to this change in the magnetic field value.

Above  $z \sim 130$  mm, the magnetic field in air in the magnet bore drops below the saturation value in the ferromagnetic Ni coating ( $B(\text{air}) < 0.6 \text{ T}$ ), cf. Fig. 5, and therefore the relative permeability of the ferromagnetic coating increases to  $\mu > 1$ . As a consequence, the stray magnetic field entering the ferromagnetic coating is suddenly strongly bent and has a discontinuous distribution and gradient.

For a quantitative estimate, we assume that the measured stray magnetic field of 0.2 T at  $z = 250$  mm enters the unsaturated magnetic coating at an angle of  $10^\circ$ . At the boundary of the coating, the field lines are bent by this  $10^\circ$  and run parallel - for some distance - to the coating surface in  $z$  direction. For  $dx$  we assume about 5 nm according to the roughness of the coating surface and we obtain for  $d\vec{B}_\perp/dx \approx 1.4 \cdot 10^6 \text{ T/m}$ . With  $v_n(\text{max}) \approx 4 \text{ m/s}$  we find for  $(d\vec{B}_\perp/dt)/B \approx 0.3 \cdot 10^8 \text{ Hz}$ . The Larmor frequency at 0.2 T is  $\omega_L = 0.4 \cdot 10^8 \text{ Hz}$ . The adiabatic condition, cf. Eq. 2, is not fulfilled here. For  $z = 400$  mm, the magnetic field in air is 6 mT and  $v_n(\text{max}) \approx 3 \text{ m/s}$ . We thus obtain  $(d\vec{B}_\perp/dt)/B \approx 10^8 \text{ Hz}$ , where  $\omega_L \approx 10^6 \text{ Hz}$ . Again, the adiabatic condition, cf. Eq. 2, is not fulfilled here.

In case the magnetic stray and holding field at larger  $z$  values is too weak to align the Weiss domains in the Ni coating, we assume  $dx$  to be of the order of the size of the Weiss domains (0.01 - 1  $\mu\text{m}$ ). Here, we obtain  $(d\vec{B}_\perp/dt)/B \approx 2 \cdot 10^8 \text{ Hz}$  (for  $v_n = 2 \text{ m/s}$  at  $z \sim 600$  mm) where the Larmor frequency, e.g., for the minimal value of the holding field,  $B(\text{min}) = 2.5 \text{ mT}$ , is about  $4 \cdot 10^5 \text{ Hz}$ . This also does not fulfill the adiabatic condition, cf. Eq. 2.

As a consequence, all UCN stored above  $z \sim 130$  mm can be rapidly depolarised already during spectral cleaning and fall into the detector. This can be seen from Fig. 6 (b) and (d): the counts with the absorber at  $z = 890$  mm and  $z = 100$  mm agree within statistics.

## 4. Conclusion

In conclusion, with these measurements we have demonstrated for the first time that in an UCN storage trap using a switchable magnetic dipole field as a shutter, UCN

with both spin orientations can be trapped: (i) Low-field seekers are accelerated away from the magnetic field and stored in the storage volume above the magnetic dipole field if their energies are below  $E = \mu \cdot B$ . (ii) High-field seekers with energies below  $E = \mu \cdot B$  are decelerated and trapped in the region of the magnetic field if they were in this region during the ramping of the magnetic field (or if they are transported adiabatically into the magnetic field region while the field is on). This phenomenon is important for UCN experiments using magnetic confinement by means of a magnetic dipole shutter. For instance in a neutron lifetime experiment it could induce a time-dependent background which may lead to a systematic shift of the measured neutron lifetime to lower values.

As a preliminary statement concerning the depolarisation probabilities  $\beta$ , we can say that these values are in the order of  $10^{-5}$  per wall bounce or smaller. Details will be described elsewhere in a forthcoming publication [16].

### **Acknowledgement**

This experiment benefited from the excellent technical support by F. Burri, D. George, A. Hirt, M. Horvath, Ph. Kaufmann, M. Negrazus, M. Sibold, R. Voegeli, V. Vrankovic (all PSI), and Th. Brenner and R. Bebb from the ILL. We thank A. Frank, V. Ignatovitch and Yu. Pokotilovskiy (all JINR Dubna), U. Schmidt (Heidelberg), and A. Steyerl (Rhode Island) for interesting discussions. The kind hospitality of ILL is gratefully acknowledged.

## References

- [1] E. Fermi and L. Marshall, Phys. Rev. 71 (1947) 666.
- [2] E. Fermi, Ricerca Scientifica 7(2) (1936) 13.
- [3] O. Halpern, M. Hammermesh, M.H. Johnson, Phys. Rev. 59 (1941) 13.
- [4] M. L. Goldberger and F. Seitz, Phys. Rev. 71 (1947) 666.
- [5] V. K. Ignatovich, The Physics of Ultracold Neutrons, Oxford Series of Neutron Scattering in Condensed Matter, vol. 5, Clarendon Press, Oxford, 1990.
- [6] R. Golub, D. J. Richardson, S. K. Lamoreaux, Ultra-Cold Neutrons, Adam Hilger, Bristol, 1991.
- [7] M. G. D. van der Grinten, J. M. Pendlebury, D. Shiers, C. A. Baker et al., Nucl. Instr. and Meth. in Phys. Res. A 423 (1999) 421.
- [8] F. Atchison, B. Blau, M. Daum, P. Fierlinger et al., Phys. Lett. B 642 (2006) 24.
- [9] F. Atchison, B. Blau, M. Daum, P. Fierlinger et al., Nucl. Instr. and Meth. in Phys. Res. B 260 (2007) 647.
- [10] K. J. Kügler, W. Paul and U. Trinks, Nucl. Instr. and Meth. in Phys. Res. A 228 (1985) 240.
- [11] W. Paul, F. Anton, L. Paul, S. Paul et al., Z. f. Physik C 45 (1989) 25.
- [12] S. Arzumanov, L. Bondarenko, S. Chernyavsky, W. Drexel et al., Phys. Lett. B 483 (2000) 15.
- [13] A. Serebrov, V. Varlamov, A. Kharitonov, A. Fomin et al., Phys. Lett. B 605 (2005) 72.
- [14] A. Pichlmaier, V. Varlamov, K. Schreckenbach, P. Geltenbort, Phys. Lett. B 693 (2010) 221.
- [15] T. Bryś, M. Daum, P. Fierlinger, P. Geltenbort et al., Nucl. Instr. and Meth. in Phys. Res. A 550 (2005) 637.
- [16] M. Daum, P. Fierlinger, B. Franke, L. Fuchs, et al., to be published.
- [17] ILL YellowBook, [www.ill.fr/YellowBook/PF2/](http://www.ill.fr/YellowBook/PF2/)

- [18] W.Drexel, Neutron News 1 (1990) 23.
- [19] A. Steyerl et al., Phys. Lett. A 116 (1986) 347.
- [20] Subrhadip Gosh, Nityananda Das and Abhijit Mookerjee, J. Phys.: Condens. Matter 10 (1998) 11773.
- [21] F. Atchison, T. Bryś, M. Daum, P. Fierlinger, Nucl. Instr. Meth. in Phys. Res. A 552 (2005) 513.
- [22] F. Atchison, T. Bryś, M. Daum, P. Fierlinger et al., Phys. Lett. B 625 (2005) 19.
- [23] F. Atchison, T. Bryś, M. Daum, P. Fierlinger, Phys. Rev. C 76 (2007) 044001.
- [24] R. Holsinger and K. Halbach, POISSON SUPERFISH code, copyright 1985-2004 by the Regents of the University of California (unpublished).

## Figure captions

### Figure 1:

Experimental apparatus for the investigation of materials for the storage of ultra-cold neutrons: 1: UCN guide from the ILL turbine; 2: beam line shutter; 3: UCN detector; 4: UCN switch between UCN guide from turbine/sample and sample/UCN detector; 5: vacuum pumping ports; 6: vertical UCN guide (sample) below magnetic field region; 7: magnet yoke; 8: magnet coils; 9: holding field coils; 10: vacuum port to prepump; 11: vacuum port to prepump; 12: vacuum pump (turbo pump); 13: extension vacuum tube; 14: vacuum sensor; 15: UCN absorber with variable height; 16: vertical UCN guide (sample) above magnetic field region (storage volume); 17: magnetic field lines at  $I = 300$  A in the air gap of the split coil magnet. Solid lines:  $B = 2.7$  T in the 30 mm air gap. Dotted lines:  $B = 1.5$  T in the center of the bore for the vertical UCN guide ( $z = 0$ ,  $r = 0$ ).

### Figure 2:

Detector counts for the sequences ‘filling’ ( $-20 - 0$  s), ‘cleaning’ ( $0 - 100$  s), ‘holding’, and ‘emptying’ for different holding times  $t_i$ ,  $t_1 - t_0 = 20$  s (top) and  $t_2 - t_0 = 320$  s (bottom);  $N_1$ ,  $N_2$  and  $N_{sp}$  are the neutron counts at  $t_1$ ,  $t_2$ , and the spin flipped neutrons, respectively. The magnetic field  $B$  at  $z = 0$ ,  $r = 0$  as a function of time is also shown.

### Figure 3:

Ultracold neutron counts as a function of the absorber height  $z$  after 20 s filling, 100 s spectral cleaning, and 20 s holding time. Black dots: integral UCN energy spectrum; open squares: differential UCN energy spectrum. The differential spectrum was obtained by the count rate differences at  $z(i)$  and  $z(i-1)$ , where  $z(i-1) = z(i) - 100$  mm. The  $z$  position for the differential spectrum is then the weighted mean,  $z(i-1) + 100/\sqrt{2}$  mm.

### Figure 4:

The potential energy in the storage volume during UCN storage as a function of the height. At small heights, the potential is mainly determined from the magnetic field in the air gap of the magnet: dotted line for HFS, dashed dotted line for LFS. The kink around 150 mm originates from saturation effects in the iron where the bore diameter increases from 81 mm to 121 mm. The gravitational potential energy (solid line) rises linearly with height and dominates at larger heights.

**Figure 5:**

Magnetic field distribution in the bore of the split coil magnet. The dark lines at  $\pm 35$  mm correspond to the inner diameter of the cylindrical vertical UCN guide.

**Figure 6:**

Comparison of the detector counts for the sample Ni/Mo alloy with weight percentages 85 (Ni) and 15 (Mo) and pure Ni with the sequences ‘filling’ ( $-20 - 0$  s), ‘cleaning’ ( $0 - 100$  s), ‘holding’ ( $100 - 245$  s), and ‘emptying’ ( $245 - 290$  s). (a) Ni/Mo data with the absorber at 890 mm. (b) Ni data with the absorber at 890 mm. (c) Ni/Mo data with the absorber at 100 mm. (d) Ni data with the absorber at 100 mm. (e) The magnetic field  $B$  at  $z = 0$ ,  $r = 0$  as a function of time. The counts in the emptying peaks in (b) and (d) agree fairly well within statistics.

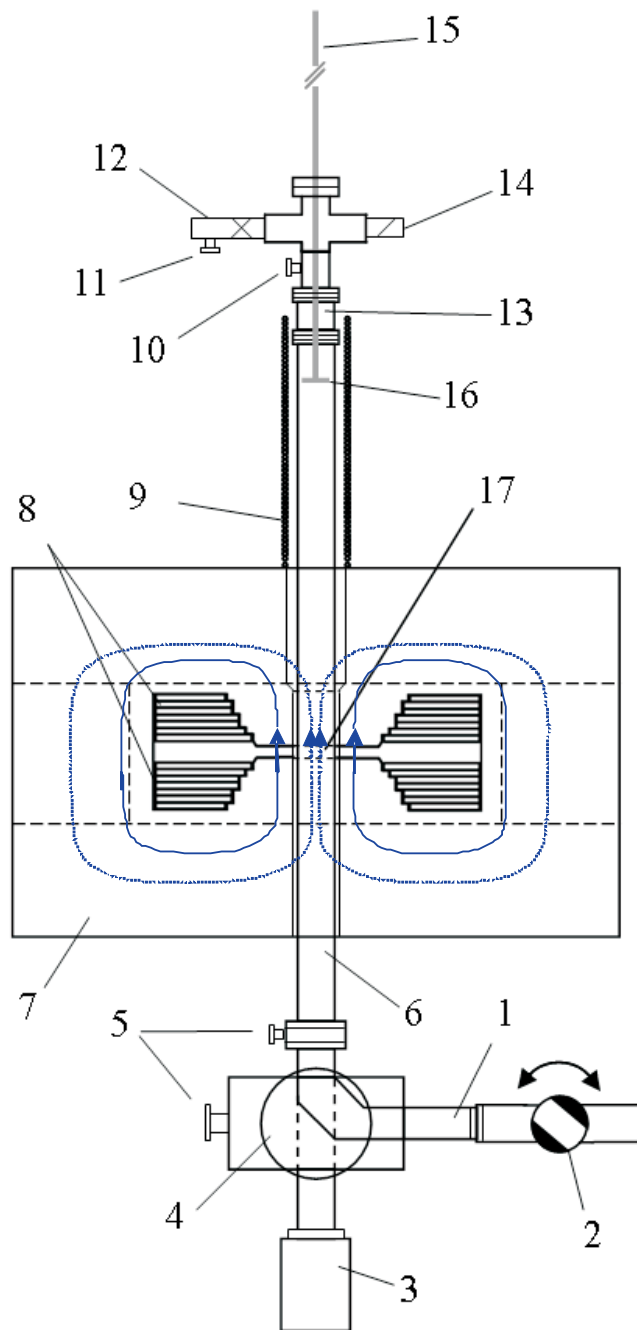


Figure 1:

Experimental apparatus for the investigation of materials for the storage of ultracold neutrons: 1: UCN guide from the ILL turbine; 2: beam line shutter; 3: UCN detector; 4: UCN switch between UCN guide from turbine/sample and sample/UCN detector; 5: vacuum pumping ports; 6: vertical UCN guide (sample) below magnetic field region; 7: magnet yoke; 8: magnet coils; 9: holding field coils; 10: vacuum port to prepump; 11: vacuum port to prepump; 12: vacuum pump (turbo pump); 13: extension vacuum tube; 14: vacuum sensor; 15: UCN absorber with variable height; 16: vertical UCN guide (sample) above magnetic field region (storage volume); 17: magnetic field lines at  $I = 300$  A in the air gap of the split coil magnet. Solid lines:  $B = 2.7$  T in the 30 mm air gap. Dotted lines:  $B = 1.5$  T in the center of the bore for the vertical UCN guide ( $z = 0$ ,  $r = 0$ ).

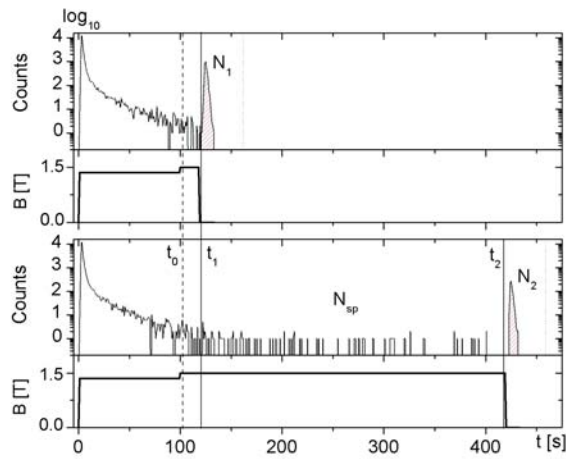


Figure 2:

Detector counts for the sequences ‘filling’ ( $-20 - 0$  s), ‘cleaning’ ( $0 - 100$  s), ‘holding’, and ‘emptying’ for different holding times  $t_i$ ,  $t_1 - t_0 = 20$  s (top) and  $t_2 - t_0 = 320$  s (bottom);  $N_1$ ,  $N_2$  and  $N_{sp}$  are the neutron counts at  $t_1$ ,  $t_2$ , and the spin flipped neutrons, respectively. The magnetic field  $B$  at  $z = 0$ ,  $r = 0$  as a function of time is also shown.

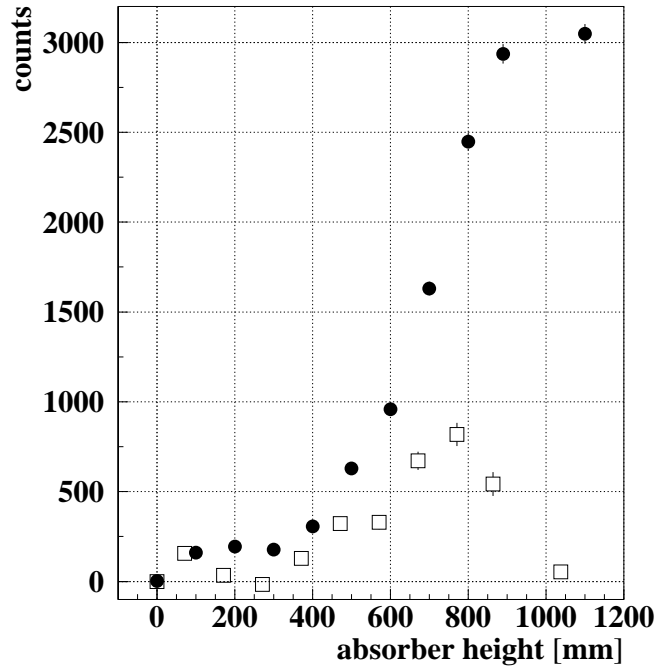


Figure 3:

Ultracold neutron counts as a function of the absorber height  $z$  after 20 s filling, 100 s spectral cleaning, and 20 s holding time. Black dots: integral UCN energy spectrum; open squares: differential UCN energy spectrum. The differential spectrum was obtained by the count rate differences at  $z(i)$  and  $z(i-1)$ , where  $z(i-1) = z(i) - 100$  mm. The  $z$  position for the differential spectrum is then the weighted mean,  $z(i-1) + 100/\sqrt{2}$  mm.

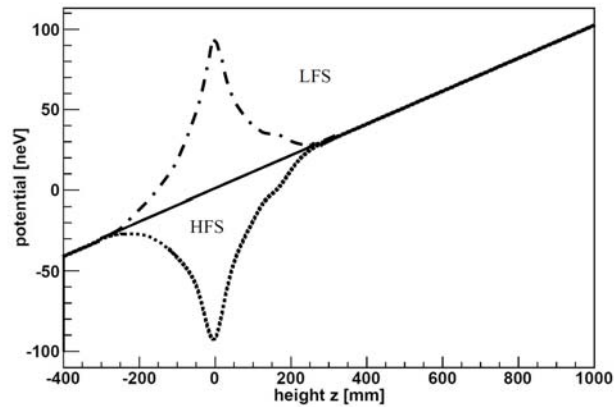


Figure 4:

The potential energy in the storage volume during UCN storage as a function of the height. At small heights, the potential is mainly determined from the magnetic field in the air gap of the magnet: dotted line for HFS, dashed-dotted line for LFS. The kink around 150 mm originates from saturation effects in the iron where the bore diameter increases from 81 mm to 121 mm. The gravitational potential energy (solid line) rises linearly with height and dominates at larger heights.

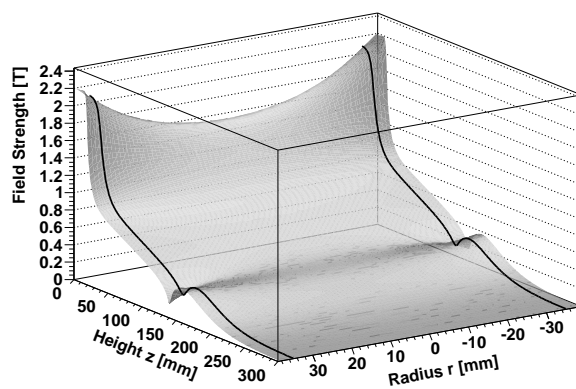


Figure 5:

Magnetic field distribution in the bore of the split coil magnet. The dark lines at  $\pm 35$  mm correspond to the inner diameter of the cylindrical vertical UCN guide.

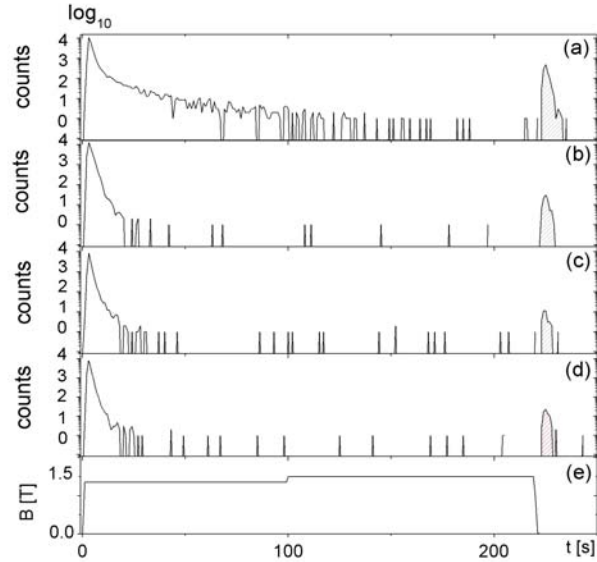


Figure 6:

Comparison of the detector counts for the sample Ni/Mo alloy with weight percentages 85 (Ni) and 15 (Mo) and pure Ni with the sequences ‘filling’ ( $-20 - 0$  s), ‘cleaning’ ( $0 - 100$  s), ‘holding’ ( $100 - 245$  s), and ‘emptying’ ( $245 - 290$  s). (a) Ni/Mo data with the absorber at 890 mm. (b) Ni data with the absorber at 890 mm. (c) Ni/Mo data with the absorber at 100 mm. (d) Ni data with the absorber at 100 mm. (e) The magnetic field  $B$  at  $z = 0, r = 0$  as a function of time. The counts in the emptying peaks in (b) and (d) agree fairly well within statistics.